The Institute of Space and Astronautical Science
Report SP No. 17 March 2003

The Aerodynamic Data Base for Asteroid Sample Return Capsule

By

Koju HIRAKI*, and Yoshifumi INATANI*

(1 February 2003)

Abstract:
The MUSES-C sample return capsule is expected to carry back to earth the collected sample from Asteroid 1998SF36 in 2007. The capsule has a blunted-cone forebody with a semi-apex angle of 45 degree, and has no active equipment for attitude control. Therefore, it should have passive aerodynamic stability all over the reentry flight. For a dispersion analysis of a landing point, it is indispensable the aerodynamic characteristics of the SRC over an entire flight regime, from rarefied gas to low-subsonic regime. The damping characteristics of the capsule over the entire flight is also required for a six-degree-of-freedom motion analysis. In the present study, the data base of the aerodynamic characteristics of the capsule were constructed by a combination of various available techniques. The source of the data were mainly obtained by a series experiments in several types of wind tunnels. Special attention was paid on the transonic damping in pitch, since it is known that a relatively flat-shaped body has a tendency of the dynamic instability in transonic regime. The grown oscillation might result in a failure of the parachute deployment. This damping-in-pitch characteristics were investigated by the special device which enabled the capsule model to rotate freely around the pitch axis in wind tunnels. A series of free-fall tests from balloons was conducted to validate the transonic and subsonic aerodynamic characteristics with emphasis on the damping-in-pitch characteristics. Another attention was paid on the damping-in-roll characterisitics to ensure the spin during the reentry. The details of the experiments and the data base were described herein.

1. INTRODUCTION

The MUSES-C program is the challenging sample return mission from Asteroid 1998SF36, which is an on-going project in ISAS, the Institute of Space and Astronautical Science (ISAS (1995)). The MUSES-C spacecraft is slated for launch in May 2003, and it will ideally pick up samples and return to earth with the collected samples in 2007. Prior to the reentry into the atmosphere, a sample return capsule will be separated from the spacecraft, with the sample canister installed inside. As shown in Fig. 1, the sample return capsule directly reenters the earth atmosphere with the speed of 11.6 km/s, spining at the rate of 0.2Hz. The spin was

* The Institute of Space and Astronautical Science, 3-1-1 Yoshinodai, Sagamihara, Kanagawa 229-8510, JAPAN.

produced by the helical-type separation spring in order to suffer the aerodynamic heating uniformly.

The MUSES-C sample return capsule has a blunted-cone forebody with a semi-apex angle of 45 degree in order to obtain higher aerodynamic drag, as shown in Fig. 2. It has no active equipment for attitude control, due to a limitation on weight and size. Therefore, the capsule itself should be aerodynamically stable over the entire reentry flight.

For a dispersion analysis of a landing point, it is indispensable the aerodynamic characteristics of the sample-return capsule over an entire flight regime, from rarefied gas to low-subsonic regime. A six-degree-of-freedom motion analysis is also quite significant for the guarantee of the successful deployment of a parachute, since the capsule is solely dependent on its passive aerodynamic stability, as is stated earlier. Therefore, the aerodynamic characteristics including stability should be provided over the entire flight regime as a data base for the analyses.

There are basically two methods to verify the aeordynamic characteristics of the capsule, the numerical and the experimental ones. Since it is known from the earlier experiences (Sammonds (1971), Krumins (1967), Uselton et al. (1972), Yoshinaga et al. (1996)) that such a body with low ballistic coefficient has a tendency to excite pitching or yawing oscillation especially in transonic range, the dynamic stability is of the special concern. The violent oscillation may cause failure of a parachute deployment, which results in a mission failure of a recovery of the sample. In this sense, the experimental approach is thought to be more reliable than the numerical one to predict the dynamic stability. Therefore, the experimental approach was adopted as long as it was possible.

In the present study, the strategy of aerodynamic data base is mainly based on the experimental data, except the low-density aerodynamics, as shown in Fig. 3. Several types of wind tunnels, from low speed to hypersonic, were used in the study. In the study of the aerodynamics of Stardust sample return capsule (Mitcheltree et. al. (1999)), the numerical approach was undertaken for the data base except for subsonic data. Since the frontal shape of Stardust sample return capsule resembles Viking probe, the most part of aerodynamic data was already compiled experimentally over 30 years. On the contrary, the capsule with the semi-apex angle of 45 degrees was not found in the previous works, and therefore the experimental data is required.

Especially, the transonic damping in pitch was the special concern, as is stated earlier, the special device was fabricated for the dynamic wind-tunnel test. The sub-scaled capsule model can rotate freely around pitch axis in the wind tunnel. Applying this device, damping-in-pitch characteristics can be obtained at each Mach number.

However, it is still insufficient to conclude the obtained damping-in-pitch characteristics to be right, since the degree of freedom is limited to one in the dynamic wind tunnel test, whereas the six degrees of freedom are allowed in the real flight. Moreover, the mass and inertia properties are different between wind-tunnel model and the real capsule. In order to validate it, balloon drop tests with full-scale models were carried out. During the free fall, the descent speed of the capsule reached maximum Mach number of approximately 1.1. During the descent, the oscillatory motion was recorded by a two-axis rate gyro installed inside.

Another attention was paid on the damping in roll characterisitics to ensure the spin during the reentry. This property should be investgated only in higher Mach numbers, since the spin is important during the high aerodynamic heating. This property was also experimentally invesigated at Mach number of 4 and 10.

In the present paper, the details of the each experiments and also the contents of the MUSES-C aerodynamic data base were described.

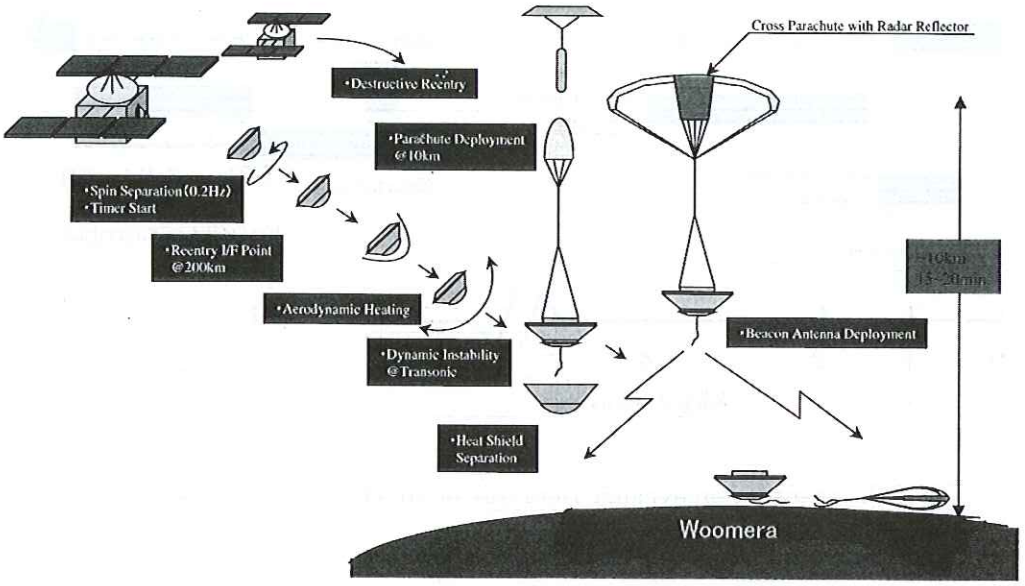

Fig. 1: Reentry Scenario of MUSES-C Sample Return Capsule.

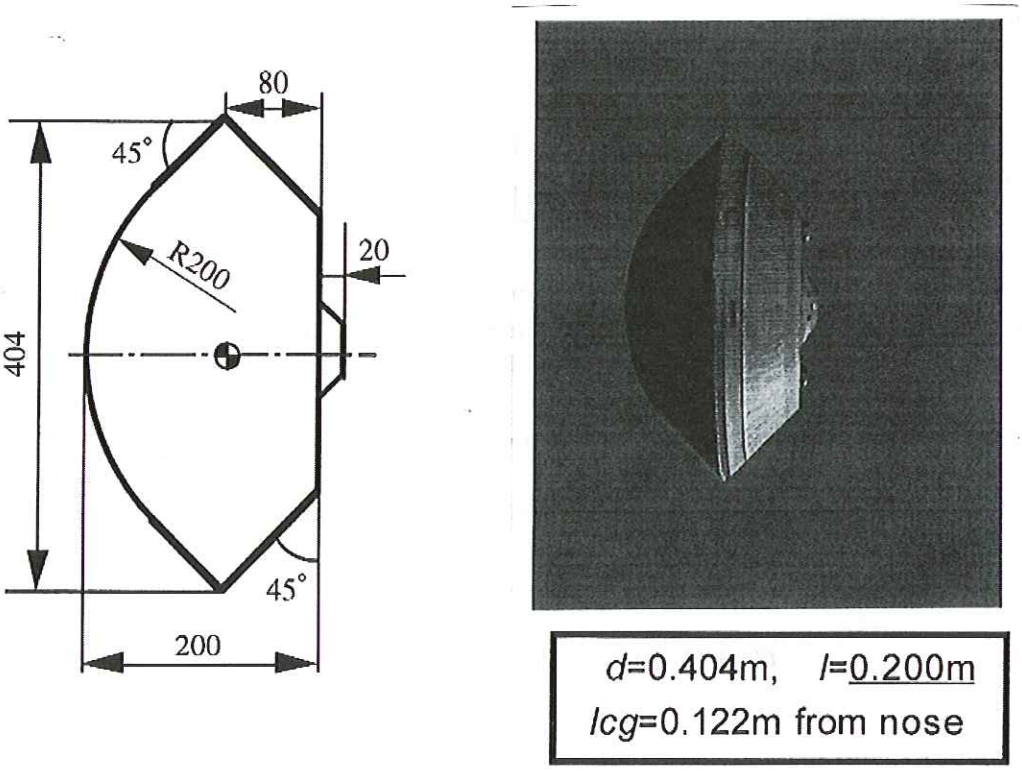

Fig. 2: Shape and dimensions of MUSES-C Sample Return Capsule.

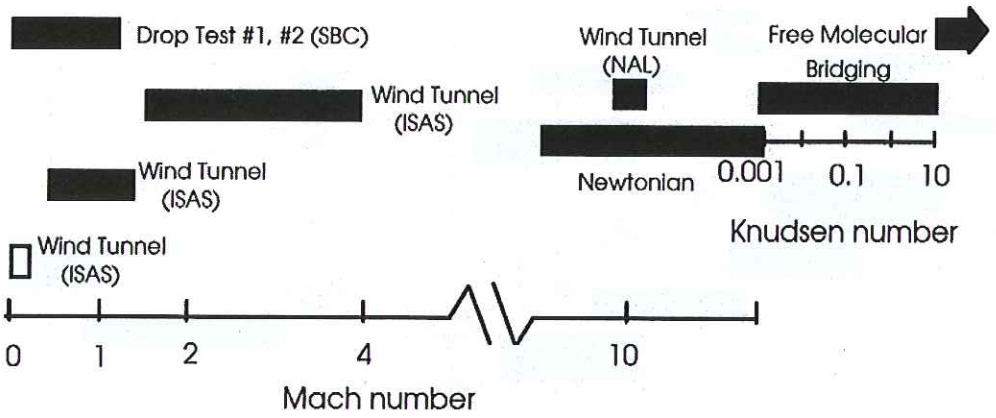

Fig. 3: Strategy of Aerodynamic Data base of MUSES-C Sample Return Capsule.

2. RAREFIED-GAS AND HYPERSONIC AERODYNAMICS

Since it is known that the simple approximation is useful for the rarefied-gas regime, the aerodynamic characteristics at low-density region was calculated instead of experiments which have difficulty in accuracy.

2.1 Calculation

Flow regimes are divided into three categories as listed in Table 1. According to the trajectory of MUSES-C sample return capsule, the region over the altitude of 123 km corresponds to free-molecular regime, and the region below the altitude of 81 km corresponds to the contiuum flow regime.

In free-molecular flow regime, the aerodynamic forces and moments were computed by integrating the effects over the descretized surface panels. The boundary condition at the surface can be selected between the specular reflection model and the diffuse reflection model. The wall temperature was assumed 300 K. For diffuse reflection, the accomodation coefficient $a_c = 1$, and for specular reflection $a_c = 0$. Experiments with carefully prepared surfaces have shown a_c to be significantly lower than 1.

For the continuum flow regime, aerodynamic forces and moments were calculated based on the modified Newtonian theroy.

In the transitional regime, the following bridging formula was applied according to Potter (1989).

$$C_t = C_c + (C_f - C_c)\ \sin^2[\frac{\pi}{8}(3 + \log K_n)] \tag{1}$$

where, C denotes the typical aerodynamic coefficient such as C_A, K_n denotes free-stream Knudsen number, and suffixes t, c, f represent transitional, continuum flow, and free molecular flow regime, respectively.

Knudsen number was calculated with following formula.

$$K_n = \frac{16}{5}\sqrt{\frac{\gamma}{2\pi}}\frac{M}{Re} \tag{2}$$

Table 1: Applied method for low-density aerodynamics.

Flow Regim	Applied Method	Knudsen Number
Free Molecular Flow Regime	Free Molecular Flow Theory	$K_n \geq 10$
Transitional Regime	Bridging Relation	$10^{-3} \leq K_n \leq 10$
Continuum Hypersonic Regime	Newtonian Theory	$K_n \leq 10^{-3}$

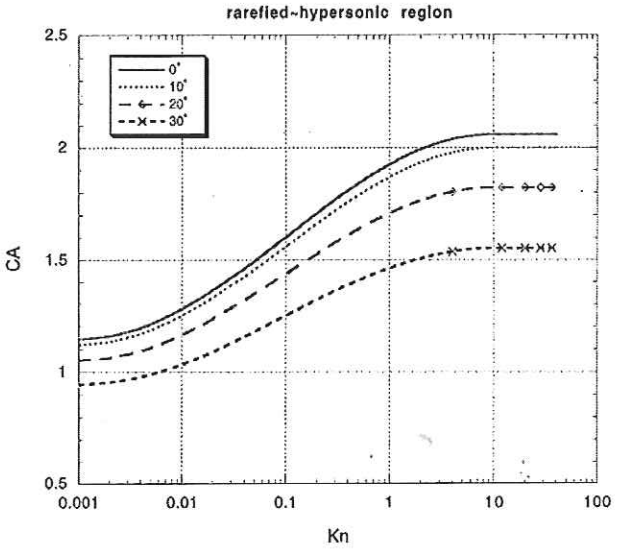

Fig. 4: Axial coefficient vs. Knudsen number.

Figs. 4 to 7 are the results of the calculation.

2.2 Hypersonic Wind-Tunnel Test

In order to validate the hypersonic static characteristics, the wind-tunnel tests were carried out in the National Aerospace Laboratory. The test conditions are summrized in Table 2. Three-component forces and moments were measured with the sting balance. Fig. 8 shows the comparison between the experimental results and the modified newtonian calculation. There are slight difference which is considered due to the base pressure, because in the newtonian calculation it assumed the base pressure equal to the free-stream static pressure. Still, the descrepancy was 2.6% of the estimated value. As for the center of pressure, good agreement can be found between them, as shown in Fig. 9.

3. SUPERSONIC AND SUBSONIC AERODYNAMICS

From low-subsonic to supersonic (up to Mach 4) flight regime, the overall wind-tunnel tests were carried out in the ISAS transonic and supersonic wind tunnels. The test condtions are

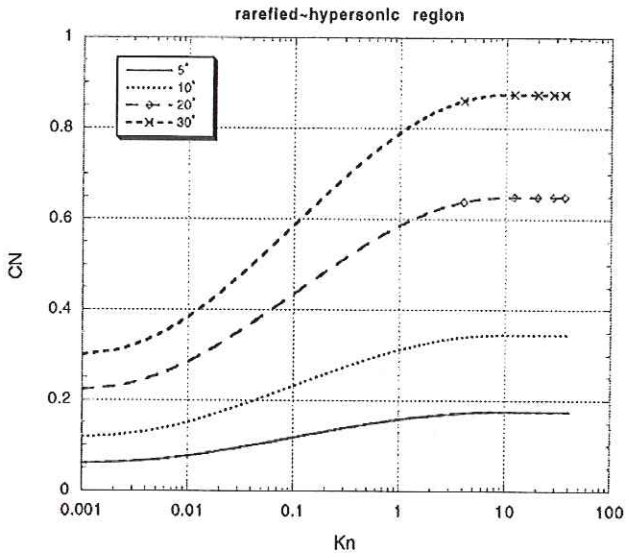

Fig. 5: Normal force coefficient vs. Knudsen number.

Table 2: Test Condition at NAL Hypersonic wind tunnel.

Mach Number	10
Stagnation Pressure	4.0MPa
Stagnation Temperature	1073K
Capsule Model Diameter	160mm

summrized in Table 3. Convetional internal six-component balance was applied in the test. In Fig. 10, the pitching moment was plotted as a function of angle of attack with the variation of Mach number. It is clear that the capsule has the static stability over the tested Mach number range, as it should be. Flow visualizations were also conducted with various schleiren techniques. Figs. 11 and 12 were obtained by color schleiren techniques(Kleine (2001)).

4. DAMPING-IN-PITCH STABILITY

4.1 Dynamic Wind-Tunnel Test

In the dynamic wind-tunnel test, free-rotation method is adopted as a dynamic test technique, which is one of the variations of the classical free oscillation method. The difference between this and classical method is in that in this method the model could rotate freely by aerodynamic moments because no constraining device such as spring is attached. In Fig. 13, the test apparatus is schematized. The model could rotate around its axis of rotation from -30 to 30 degrees in a pitch plane, which is sustained aft by strut support through a pair of ball bearings in order to reduce friction as minimum as possible. The position of center of gravity of the movable parts is adjusted to coincide to that of axis of rotation in order not to produce any

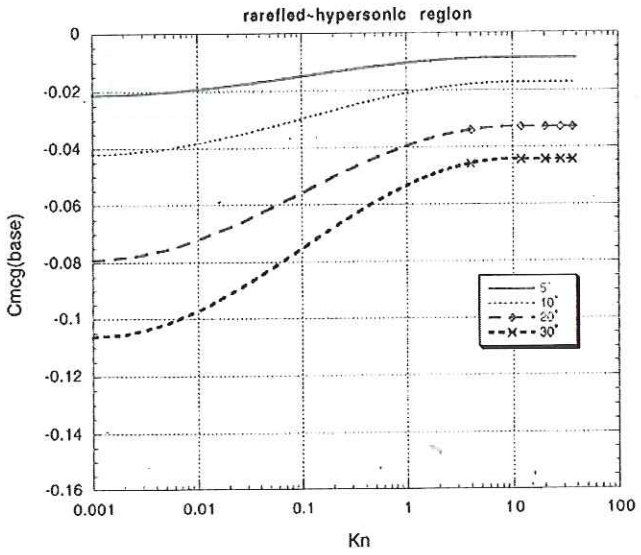

Fig. 6: Pitching Moment coefficient vs. Knudsen number (Xcg=0.122m from nose).

moment around it due to C.G. offset. The stopper device is installed inside of the sting support to keep the zero angle-of-attack condition until the free stream is established. Once the flow is established, the stopper is released electronically and the model starts to rotate simply by aerodynamic moment. The motion of the model is detected by the potentiometer attached at the axis of rotation. The output signal from potentiometer and the stopper-release status signal are amplified and converted to digital signals in the A/D converter, simultaneously.

Applying this devise to the wind tunnel test at each Mach number, the oscillatory motion in the angle of attack is obtained. As is stated earlier, in the transonic region, the blunt-body capsule shows the self-excited oscillation, even if it is statically stable. This is due to the inherent dynamic instability of the capsule. Fig. 14 shows the typical self-excited oscillation due to the dynanmic instability.

From the time history of the oscillatory motion of the model, damping-in-pitch characteristics is obtained at each Mach number, by giving a simple curve fit to the data (Hiraki (1997)).

$$\ddot{\alpha} - \frac{qSd^2}{IV} \cdot \epsilon \left\{ 1 - \frac{\alpha^2}{\delta^2} \right\} \cdot \dot{\alpha} + \frac{qSd}{I} \cdot \left(a + b\alpha^2 \right) \cdot \alpha \tag{3}$$

where, V: free-stream velocity, d: model diameter,ϵ, δ, a, b :constants.

Fig. 15 shows the typical result of the fitting based on the above expression to the experimental data at $M = 1.3$. Applying this method to various Mach number, the damping-in-pitch characteristics are obtained, as shown in Fig. 16. Conversely, using this damping-in-pitch characteristics the oscillatory motion can be reproduced. Futhermore, applying this method, the oscillatory motion of the real capsule can be predicted.

However, it is still insufficient to conclude the obtained damping-in-pitch characteristics to be right. Since the degree of freedom is limited to one in the dynamic wind tunnel test, whereas the six degrees of freedom are allowed in the real flight. Moreover, the mass and inertia

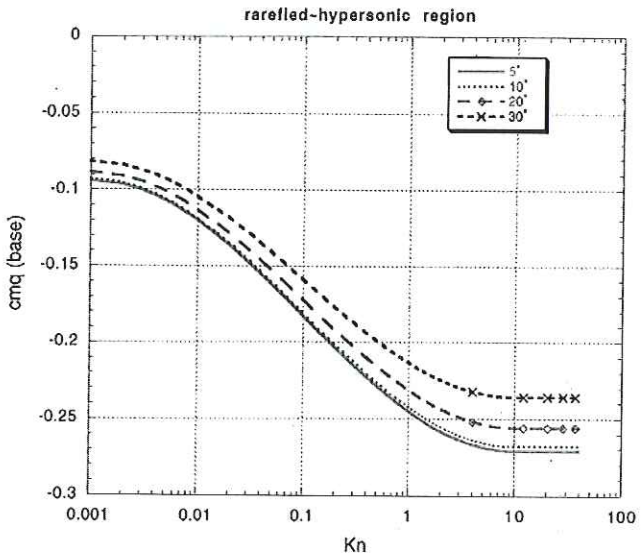

Fig. 7: Damping-in-pitch coefficient vs. Knudsen number.

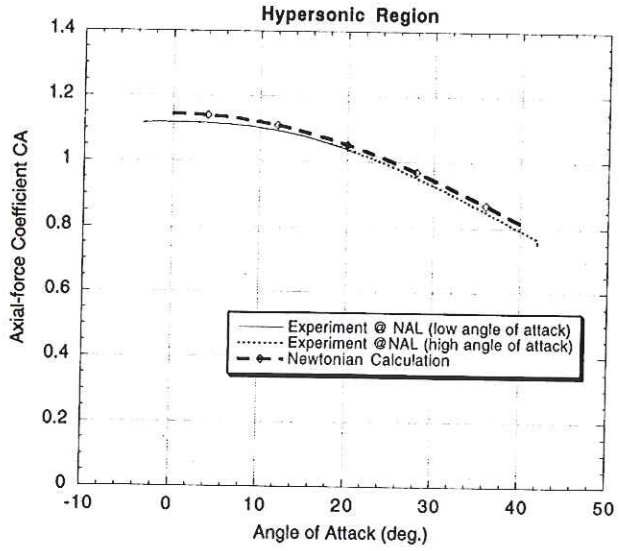

Fig. 8: Comparison of axial-force coefficient between experiments and newtonian calculation.

properties are different between wind-tunnel model and the real capsule. This point will be discussed in the later section.

The identical free-rotational device was used also in NAL hypersonic wind tunnel. This time, the initial angle of attack was set to 10 degrees to validate its dynamic stability. At $M = 10$, the capsule showed its negativokae damping and decreased its angle of attack, as shown in

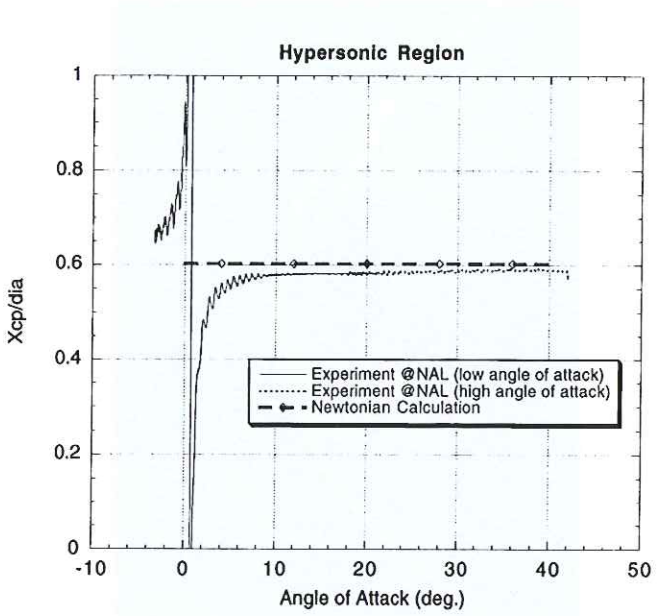

Fig. 9: Comparison of center-of-pressure location between experiments and newtonian calculation.

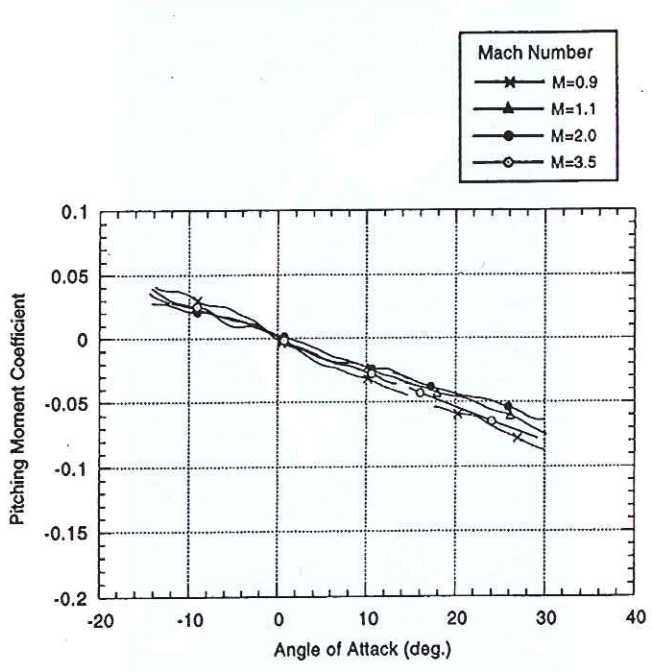

Fig. 10: Pitching moment slope (Xcg=0.122m from nose).

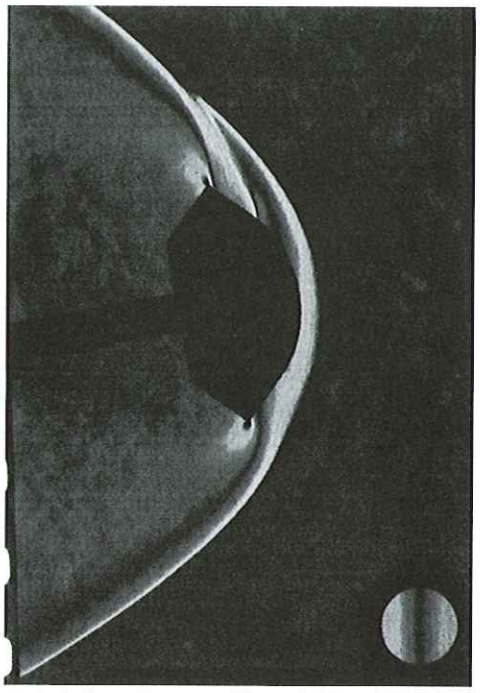

Fig. 11: Flow visualization with magnitude-indicating color mask(vertical layout) at $M = 3.0$ and $\alpha = 10deg.$.

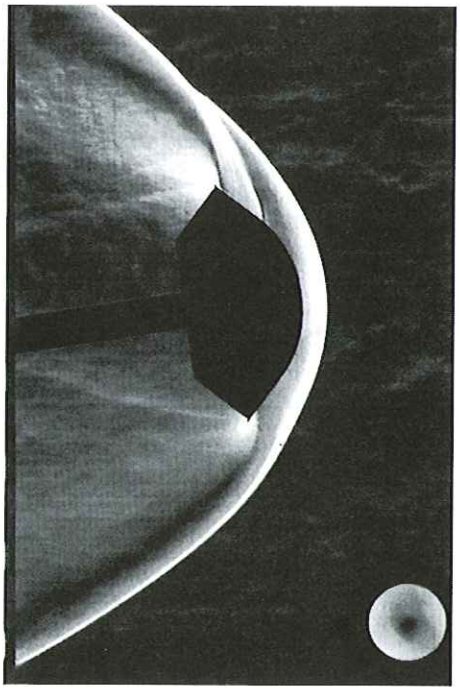

Fig. 12: Flow visualization with direction-indicating color mask at $M = 3.0$ and $\alpha = 10deg.$

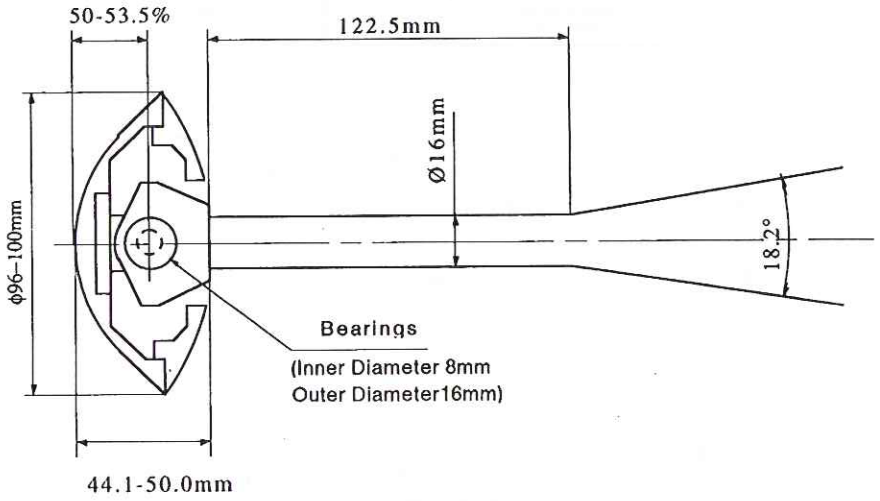

Fig. 13: Test apparatus.

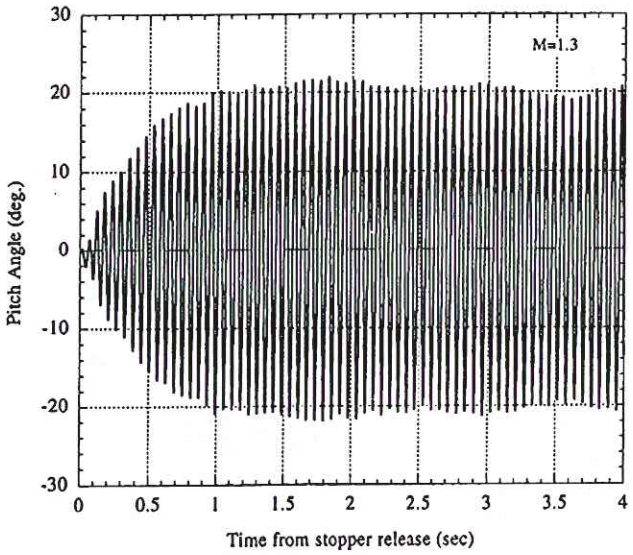

Fig. 14: Typical self-excited oscillation at $M = 1.3$.

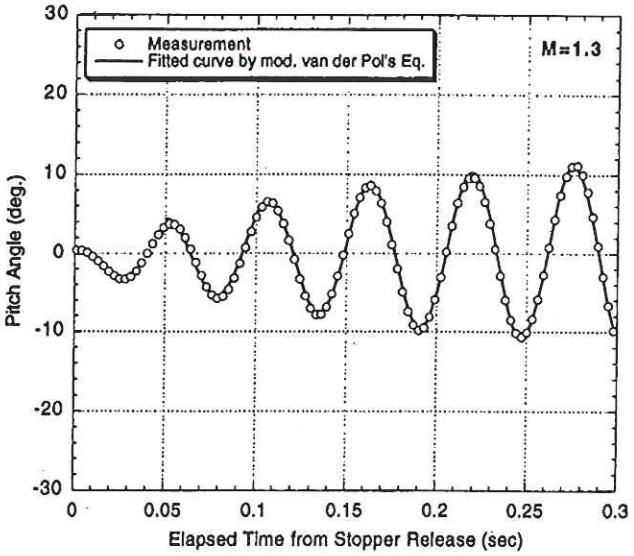

Fig. 15: Comparison of the curve-fit and the experimental oscillation at $M = 1.3$

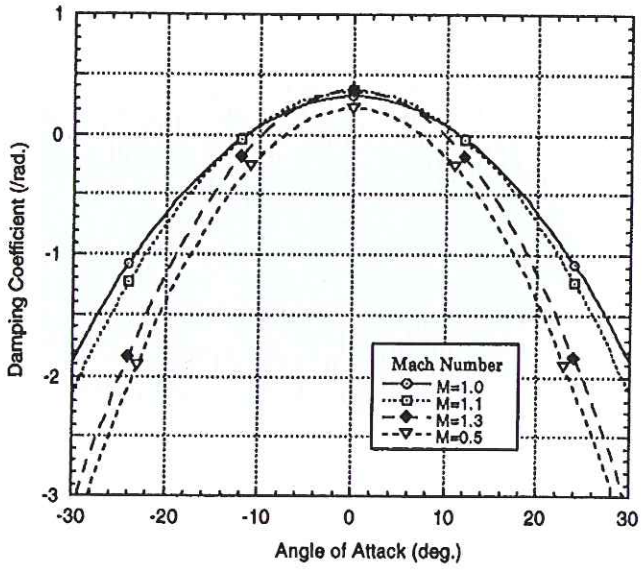

Fig. 16: Obtained damping-in-pitch coefficients by the curve-fit.

Table 3: Test Conditions at ISAS transonic and supersonic wind tunnel.

Mach Number	Angle of Attack (deg.)	Dynamic Pressure (kg/cm^2)	Reynolds number
0.3	-15∼15	0.091	0.68×10^6
	15∼35	0.106	0.81×10^6
0.5	-15∼15	0.221	1.05×10^6
	15∼35	0.265	1.26×10^6
0.7	-15∼15	0.369	1.33×10^6
	15∼35	0.443	1.60×10^6
0.9	-15∼15	0.503	1.52×10^6
	15∼35	0.590	1.81×10^6
1.0	-15∼15	0.557	1.59×10^6
	15∼35	0.669	1.90×10^6
1.1	-15∼15	0.600	1.62×10^6
	15∼35	0.720	1.95×10^6
1.2	-15∼15	0.630	1.64×10^6
	15∼35	0.751	1.97×10^6
1.3	-15∼15	0.646	1.65×10^6
	15∼35		
1.5	-15∼15	0.937	2.47×10^6
	15∼35	0.940	2.45×10^6
2.0	-15∼15	0.819	2.20×10^6
	15∼35	0.821	2.20×10^6
2.5	-15∼15	0.819	2.42×10^6
	15∼35	0.820	2.43×10^6
3.0	-15∼15	0.792	2.70×10^6
	15∼35	0.792	2.71×10^6
3.5	-15∼15	0.501	2.02×10^6
	15∼35	0.502	2.03×10^6
4.0	-15∼15	0.410	1.97×10^6
	15∼35	0.410	1.98×10^6

Fig. 17. From this result, it is considered that the angle of attack during the hypersonic flight will be damped well.

4.2 Varidation by Balloon Drop Test

In order to verify the discussions described in earlier sections, free-flight test with real size capsule is carried out(Hiraki (1997)). In a free-flight test, the degree of freedom is six, as not in the case of wind tunnel test. The capsule has a similar shape but different in size and mass property, such as weight and moment of inertia. It is lifted up to 36 km in altitude by a balloon with $30,00m^3$ from Sanriku Balloon Center, and then separated from gondola by a command from GSE. During the descent, the flight Mach number exceeds unity, where the dynamic instability is expected to be severest. Inside the capsule two-axis rate sensor is on-board, and angular rates in pitch and yaw are directly measured. In addition, as CCD camera is also installed in rearside of the capsule, the attitude during descent could be known from the traces

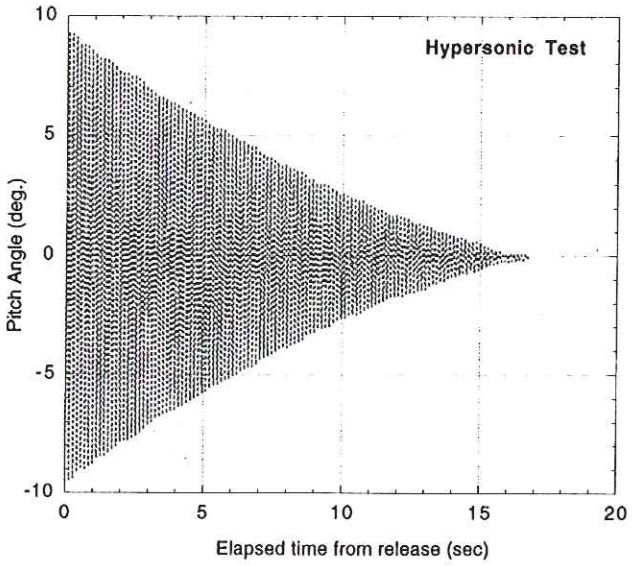

Fig. 17: Damping-in-pitch.

of balloon and Sun on the images taken by it.

Flight environment, such as Mach number and dynamic pressure is presented in Fig. 18 as a function of time counted from separation. The maximum Mach number established is approximately 1.1, at around 45 seconds from separation. As shown in it, flight Mach number and dynamic pressure varies as time increases, whereas they remain constant during the blow in the wind tunnel test.

The time history of total angle of attack derived from CCD images is diagrammed in Fig. 19. In order to reduce the effort of derivation minimum only a limited history during one cycle of oscillation at a certain interval of time is presented, which is denoted by a solid circle in the figure. The solid line is illustrated for help of understandings, which is representing the envelope of the time history. The maximum value is achieved not at maximum Mach number but after the dynamic pressure exceeds its peak.

In Fig. 20, the predicted angle of attack is presented, which was based on the experimental data obtained in the wind tunnel. The comparison between Fig. 19 and 20 shows good agreement in terms of the amplitude of the oscillation. From this fact, it is safely concluded that the presented method based on the wind-tunnel data is reliable also for the full-size and muti-freedom flight.

5. DAMPING-IN-ROLL STABILITY

Another attention was paid on the damping-in-roll characteristics in terms of spin motion which should be maintained during the reentry in order to average the aerodynamic heating. The spin was initiated by the separation spring at the separation from the spacecraft. The spin rate is estimated at about 0.2 Hz. If the sample return capsule has a strong damping in roll, then the spin motion will be terminated by the aerodynamic force.

In order to investigate this damping-in-roll characteristics, special device was fabricated for wind-tunnel tests, as shown in Fig. 21. The capsule model was initially rotated around

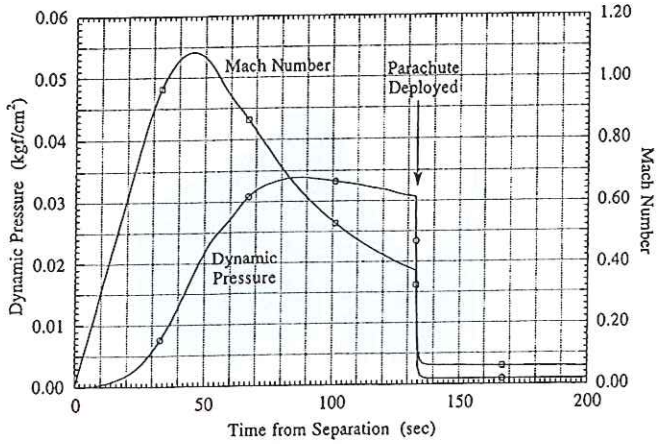

Fig. 18: Mach number and dynamic pressure during descent in free-flight test.

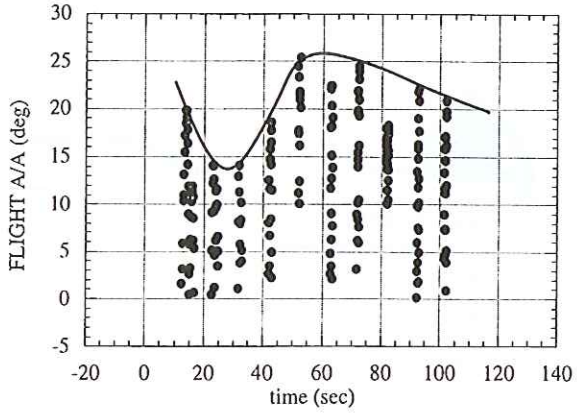

Fig. 19: Total angle of attack derived from CCD image in free-flight test.

roll axis by the compressed air flow transmitted from N_2 bottle. After it achieves the desired spin rate, the wind-tunnel was started to establish the flow. The spin rate was monitored by the laser detector. The time history of the spin gives the information of the damping-in-roll characteristics.

From the time constant of the decay of the spin rate, the damping-in-roll coefficient can be estimated.

$$I\dot{\omega} + \frac{\rho V S d}{4} C_{lp}\,\omega + N(W) = 0 \tag{4}$$

where, I: moment of inertia around spin axis, ρ: density of air, ω: angular velocity, C_{lp}: damping-in-roll coefficient, N:friction due to drag. The friction component was estimated experimentally by adding various level of loads. According to above expression, the estimated damping-in-roll coefficient was in the range of $-0.012 \leq -C_{lp} \ll -0.007$, as shown in Fig. 22. In the figure, only the absolute value of the damping-in-roll coefficient was described. This test was conducted at $M = 4.0$.

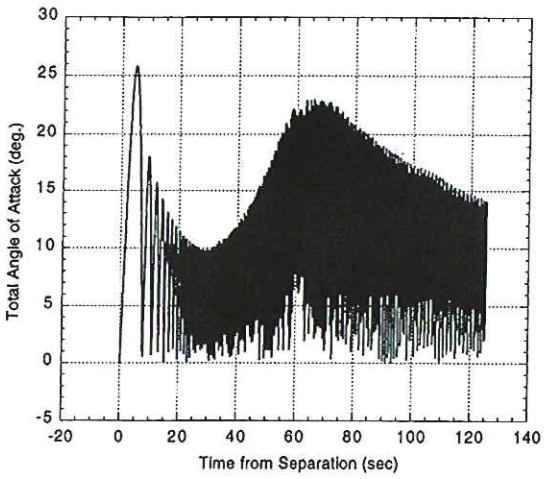

Fig. 20: Predicted total angle of attack history based on the wind-tunnel test.

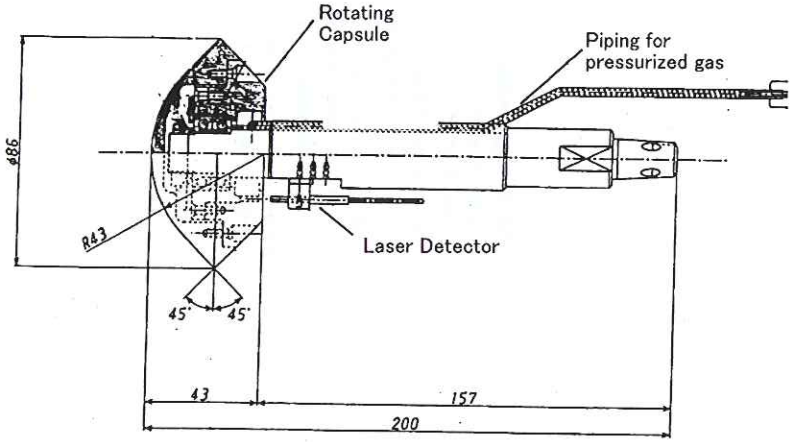

Fig. 21: Test device for damping-in-roll characteristics in wind tunnel.

6. AERODYNAMIC DATA BASE

All the data obtained by a series of experiments and by simple calculation were compiled to construct the overall aerodynamic data base for MUSES-C sample return capsule. Fortran subrotuine style was selected.

Input variables for the subroutine are as follows;

Velocity (m/s)

Angle of attack (deg.)

Atmospheric density (kg/m^3)

Atmospheric temperature (K)

Diameter of sample return capsule (m)

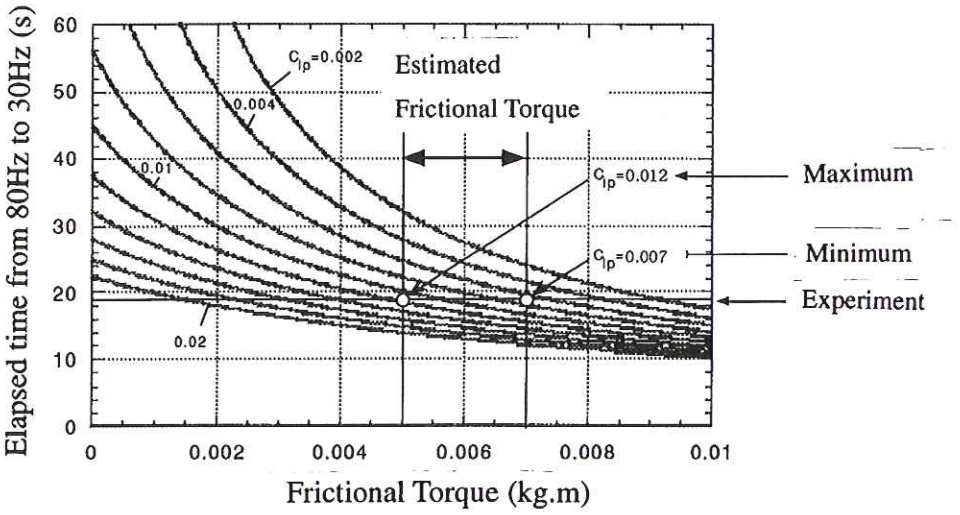

Fig. 22: Chart for estimation of damping-in-roll coefficient from experimental decay data of spin.

Position of C.G. measured from top (m)
Outputs are;

C_A Axial Coefficient

C_N Normal Force Coefficient

C_D Drag Coefficient

C_L Lift Coefficient

Cm_{cg} Pitching Moment Coefficient around C.G. (reference length=diameter)

Cm_q Damping in Pitch Coefficient (reference length=diameter)

Cl_p Damping in Roll Coefficient (reference length=diameter)

The axial-force coefficient derived from the data base is typically depicted in Fig. 23.

7. LIMITATION AND NOTES FOR USE

Here are described the limitaions and notes on the Aerodynamic Data Base for MUSES-C sample return capsule;

- Range of angle of attack is limited to 35 degree. Beyond it, the coefficients remain constant.
- Position of center of gravity is insesitive to damping characteristics.
- Linear interpolatoin is applied.

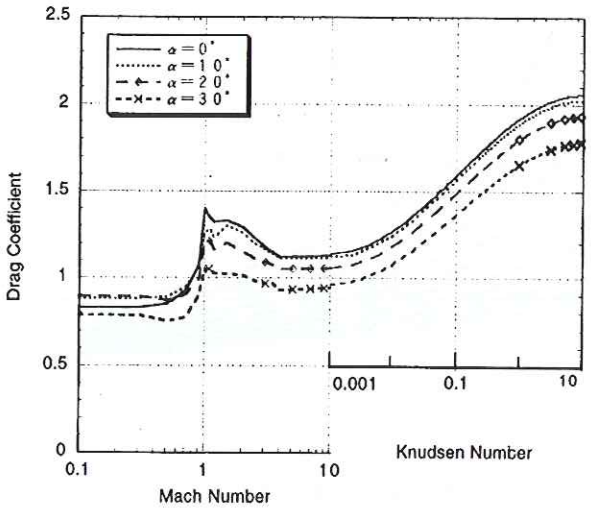

Fig. 23: Axial coefficient output.

8. CONCLUSION

The data base of the aerodynamic characteristics of the MUSES-C sample return capsule were constructed by a combination of various available techniques. The source of the data were mainly obtained by a series experiments in several types of wind tunnels. Special attention was paid on the transonic damping in pitch, since it is known that a relatively flat-shaped body has a tendency of the dynamic instability in transonic regime. The data obtained in the transonic wind tunnels were validated by a series of balloon-drop tests. Another attention was paid on the damping-in-roll characteristics in terms of spin motion which should be maintained during the reentry in order to average the aerodynamic heating. All the data were compiled in the form of "Aerodynamic data base for MUSES-C sample return capsule", which can be used as Fortran subroutine for 6-DOF motion analysis.

ACKNOWLEDGMENT

The author wishes to express his deep appreciation to Mr. Sato for his dedicated test support, and also to Mr. Niwa for his great help for the dynamic test device. He also expresses gratitude to Mr. Hirabayashi, Mr. Sekine, Mr. Koyama at NAL Hypersonic Wind tunnel for their test support. The author also thanks Dr. Izutsu for his effort to conduct supersonic wind-tunnel tests, and also thanks Mr. Hongoh for his effort to conduct the roll-damping wind tunnel test at ISAS and data reduction. Mr. Honda and Ms. Fukunaga of IHI Aerospace Company conducted the calculation of the low-density aerodynamics. The balloon drop tests were planned and carried out by ISAS capsule team and ballooning team. The flow visualizations of Figs. 11 to 12 were obtained in a collaboration with Dr. H.Kleine, Tohoku University (present address: University of New South Wales/Australian Defence Force Academy, Canberra, Australia)

REFERENCES

Working Group of Asteroid Exploration Mission, 1995, Proposal for Asteroid Exploration Mission (MUSES-C), The Institute of Space and Astronautical Science.

Sammonds R. I., 1971, Dynamics of High-Drag Probe Shapes at Transonic Speeds, NASA TN D-6489.

Krumins M. V., 1967, A Ballistic Range Study of Aerodynamic Characterestics of Mars Probe/Lander Shapes, AIAA Paper 67–167.

Uselton, B. L., and Wallace, A. R., 1972, Damping-in-Pitch and Drag Characteristics of the Viking Configuration at Mach Numbers from 1.6 through 3, AEDC-TR-72-56.

Yoshinaga, T., Tate, A., Watanabe, M. and Shimoda, T., 1996, Orbital Re-Entry Experiment Vehicle Ground and Flight Dynamic Test Results Comparison, Journal of Spacecraft and Rockets, Vol.33, No.5, pp. 635–642.

Mitcheltree, R. A., Wilmoth, R. G., Cheatwood, F. M,, Brauckmann, G. J. and Greene, F. A., 1999, "Aerodynamics of Stardust Sample Return Capsule", Journal of Spacecraft and Rockets, Vol.36, No.3, pp. 429–435.

Wilmoth, R. G., Mitcheltree, R. A., and Moss, J. N., 1999, "Low-Density Aerodynamics of the Stardust Sample Return Capsule", Journal of Spacecraft and Rockets, Vol.38, No.3, pp. 436–441.

Potter, J. L., "Procedure for Estimating Aerodynamics of Three-Dimensional Bodies in Transitional Flow", *Rarefied Gas Dynamics: Threoretical and Cumputational Techniques*, edited by E. P. Muntz, 1989 D. P. Weaver, and D. H. Campbell, Vol.118, Progress in Astronautics and Aeronautics, AIAA, Washington, DC.

Kleine, H., 2001, "Flow Visualization", Chapter 5.1 in: "Handbook of Shock Waves", Academic Press, Volume 1, pp. 683–740.

Hiraki, K., 1997, Experimental Study on Dynamic Instability of Capsule-type Body, Ph.D Thesis, University of Tokyo.